ACS APPLIED MATERIALS & INTERFACES

RESEARCH ARTICLE

www.acsami.org

Polydimethylsiloxane as a Macromolecular Additive for Enhanced Performance of Molecular Bulk Heterojunction Organic Solar Cells

Kenneth R. Graham,[†] Jianguo Mei,[†] Romain Stalder,[†] Jae Won Shim,[‡] Hyeunseok Cheun,[‡] Fred Steffy,[§] Franky So,[*,§] Bernard Kippelen,[*,‡] and John R. Reynolds[*,†]

[†]The George and Josephine Butler Polymer Research Laboratory, Department of Chemistry and Center for Macromolecular Science and Engineering, University of Florida, Gainesville, Florida 32611-7200, United States

[‡]School of Electrical and Computer Engineering and Center for Organic Photonics and Electronics, Georgia Institute of Technology, 777 Atlantic Drive, Atlanta, Georgia 30332, United States

[§]Department of Materials Science and Engineering, University of Florida, Gainesville, Florida 32611, United States

Supporting Information

ABSTRACT: The effect of the macromolecular additive, polydimethylsiloxane (PDMS), on the performance of solution processed molecular bulk heterojunction solar cells is investigated, and the addition of PDMS is shown to improve device power conversion efficiency by ~70% and significantly reduce cell-to-cell variation, from a power conversion efficiency of 1.25 ± 0.37% with no PDMS to 2.16 ± 0.09% upon the addition of 0.1 mg/mL PDMS to the casting solution. The cells are based on a thiophene and isoindigo containing oligomer as the electron donor and [6,6]-phenyl-C61 butyric acid methyl ester ($PC_{61}BM$) as the electron acceptor. PDMS is shown to have a strong influence on film morphology, with a significant decrease in film roughness and feature size observed. The morphology change leads to improved performance parameters, most notably an increase in the short circuit current density from 4.3 to 6.8 mA/cm^2 upon addition of 0.1 mg/mL PDMS. The use of PDMS is of particular interest, as this additive appears frequently as a lubricant in plastic syringes commonly used in device fabrication; therefore, PDMS may unintentionally be incorporated into device active layers.

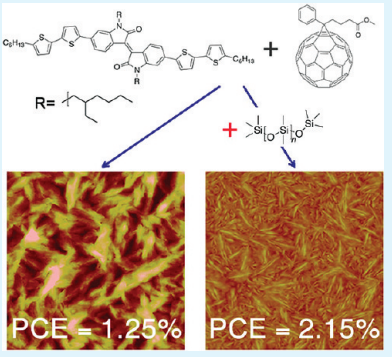

KEYWORDS: bulk heterojunction, organic solar cell, molecular photovoltaic cell, morphology control, additive processing

INTRODUCTION

The development of affordable solar energy remains a field of intense research interest and commercial development.[1] One promising low-cost solar energy technology is organic bulk heterojunction (BHJ) solar cells.[2−6] In contrast to traditional inorganic solar cells, organic BHJ solar cells can be solution processed allowing for potentially large scale and inexpensive fabrication on flexible substrates.[7] Critical to the efficient operation of BHJ solar cells is the nanoscale phase separated morphology consisting of electron-donating and electron-accepting phases.[2] This morphology can be altered and the BHJ solar cell efficiency increased through techniques such as thermal annealing,[3] solvent annealing,[8] and the use of solvent additives.[9]

Primarily, research on organic BHJ solar cells has focused on polymer:fullerene blends with current power conversion efficiencies (PCEs) exceeding 6% in small area devices.[5,10] Recently, there have also been significant advances in the development of solution processed molecular BHJ solar cells with efficiencies predominantly in the 1.5−3% range.[6,11−20] Although these molecular BHJ solar cells are currently less efficient than their polymeric counterparts, they possess several inherent advantages including more well-defined chemical structures, simpler purification methods, easier modification and functionalization, no end group contaminants, and more reproducible synthesis. In raising the efficiencies of these molecular BHJ solar cells, the Nguyen group has developed several diketopyrrolopyrrole (DPP) based donor−acceptor−donor oligomers with PCEs exceeding 4% for the most efficient cells.[6,11,16] These results suggest that molecular BHJ solar cells have the potential to reach efficiencies comparable to their polymeric counterparts.

The performance of BHJ solar cells is strongly dependent on the ability of the cells to efficiently dissociate excitons and transport charges to the electrodes.[4,21] To achieve efficient exciton dissociation the donor and acceptor (D and A) phase sizes must be sufficiently small (10−20 nm) to allow for generated excitons to diffuse to a donor−acceptor interface.[4,22,23] Additionally, a bicontinuous network of donor and acceptor phases must exist with sufficiently high mobility to allow for efficient charge transport to the electrodes.[21] Several different strategies and techniques have been applied to achieve a more desirable morphology such as thermal annealing,[3,24] solvent vapor annealing,[8,25] and the use of solvent additives.[9,19,26−32] In general these techniques increase the degree of D and A phase separation and lead to more ordered

Received: January 10, 2011
Accepted: March 15, 2011
Published: March 15, 2011

Scheme 1. Molecular structure of thiophene and isoindigo containing oligomers

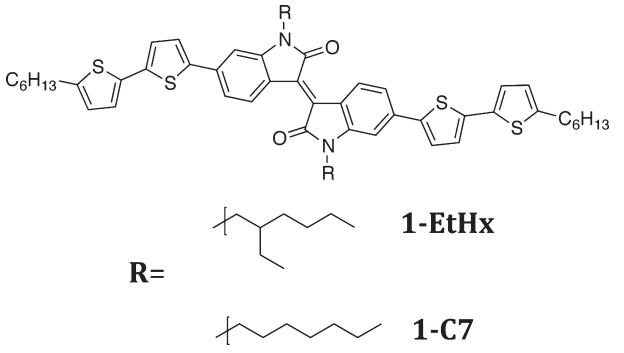

D and A phases, thereby enhancing charge transport and reducing charge recombination.

The incorporation of solvent additives has been shown to be an effective method to improve device performance, while also reducing or eliminating the need for postproduction treatments such as thermal or solvent annealing.[9,19,26−32] As a general guideline for selecting solvent additives, the additive should be less volatile than the parent solvent and have a higher solubility for PCBM than the polymer.[26,27] It has been proposed that these less volatile solvent additives function by selectively solubilizing the PCBM component, resulting in aggregation of the polymer during the film drying process.[26,27] This increased polymer aggregation leads to the formation of more highly ordered D and A phases, thus improving device performance. The use of poor solvent additives for both poly(3-hexylthiophene) and PCBM has also been demonstrated to improve BHJ solar cell performance by increasing aggregation and resulting in increased D−A phase separation.[32]

Herein we present the use of polydimethylsiloxane (PDMS) as a macromolecular additive to increase the performance of molecular BHJ solar cells based on a previously reported thiophene and isoindigo containing oligomer blended with [6,6] phenyl-C61-butyric acid methyl ester ($PC_{61}BM$). To the best of our knowledge, a macromolecular additive has not previously been reported to improve organic BHJ solar cell performance, and with the exception of one recent article the use of additives has not been applied to molecular BHJ solar cells.[19] It is demonstrated that the addition of 0.1−0.75 mg/mL PDMS to the spin-casting solution has a beneficial effect on device morphology that results in an increased power conversion efficiency and improved cell-to-cell reproducibility. Additionally, PDMS decreases the need for thermal annealing, as a drastic improvement in efficiency for nonthermally annealed devices upon addition of PDMS is observed. Due to the subtleties of the results, the experiments were repeated in three different laboratories. Although the results showed significant variation, an improvement in cell-to-cell reproducibility and/or an increase in average cell performance upon the addition of PDMS were observed in all laboratories.

RESULTS AND DISCUSSION

The molecular BHJ solar cells reported herein are based on a previously published thiophene and isoindigo containing oligomer as shown in Scheme 1.[33]

In our previously published work, we reported an efficiency of 1.76% that was obtained using plastic syringes to dispense the active layer solutions onto the poly(ethylene dioxythiophene):poly(styrene sulfonate) (PEDOT:PSS) coated indium tin oxide (ITO) on glass substrate followed by thermal annealing at 100 °C.[33] Upon switching to glass syringes a drop in PCE to 1.25% was observed (see the Supporting Information, Figure S1). Through a detailed investigation it was determined that the plastic syringes contained PDMS that was being incorporated into our active layer during the fabrication procedure. The identity of this compound as PDMS was confirmed by MALDI-MS and IR spectroscopy (see the Supporting Information, Figures S2 and S3).

To verify that PDMS was responsible for the enhanced efficiencies, solar cells were prepared with known concentrations of PDMS added to the active layer solutions. The devices were prepared by using a clean glass syringe to deposit the **1-EtHx**:$PC_{61}BM$ (1:1) or **1-C7**:$PC_{61}BM$ (1:1) chlorobenzene solutions onto the PEDOT:PSS coated ITO. The solutions were spin-cast and the devices were completed by thermal deposition of a Ca/Al top electrode. The results reproducibly indicate a ∼70% increase in efficiency (from 1.25 to 2.15%) upon incorporation of PDMS (in the Reynolds laboratory) at concentrations ranging from 0.10 to 0.75 mg/mL as shown in Figure 1 and Table 1. The effect of PDMS on these devices was also tested in the Kippelen and So laboratories. Results obtained in the So laboratory were similar to the results obtained in the Reynolds laboratory; however, results obtained in the Kippelen laboratory differed (see the Supporting Information, Figure S4). Results obtained in all laboratories indicate a decrease in cell-to-cell variation and/or an improvement in PCE along with a change in morphology upon the addition of PDMS. It is likely that small differences in processing conditions are contributing to the different results obtained between laboratories.

Figure 1b and Table 1 indicate that the increase in PCE is primarily attributed to an enhancement in current density; however, all of the other critical parameters also show an improvement upon incorporation of PDMS. In addition to an increase in PCE, PDMS also helps to improve cell consistency as evident by the larger standard deviation associated with the cells containing no PDMS. A consistent PCE (∼2.15%) is observed when between 0.1 and 0.75 mg/mL of PDMS are added to the solutions, indicating the cells are not overly sensitive to PDMS concentration. However, it should be noted that results obtained in the Reynolds laboratory deviated from those obtained in the So and Kippelen laboratories. For devices fabricated and tested in the So labarotory, PCEs of 1.42 ± 0.09, 2.08 ± 0.17, and 1.80 ± 0.11 were measured for devices with 0, 0.1, and 0.3 mg/mL PDMS respectively. For devices fabricated in the Kippelen laboratory, the yield of devices without PDMS was very low due to significant inhomogeneities in the **1-EtHx**:$PC_{61}BM$ films. Out of 10 devices, only six devices yielded measurable current−voltage characteristics with PCEs ranging between 0.36 and 1.84% with an average value of 0.99%. In contrast, the yield for 10 devices for each PDMS concentration was 100% and the standard deviation in PCE was less than 0.1%. The measured average PCE was 1.51 ± 0.10, and 1.46 ± 0.06 in devices with 0.1, and 0.3 mg/mL PDMS, respectively. It should be noted that changes in the values of the PCEs measured in all three laboratories may be attributed to differences in the spectrum of the AM 1.5 solar simulators.

Absorbance measurements of the **1-EtHx**:PCBM films show a very broad absorbance spanning the entire visible region up to ∼700 nm as shown in Figure 2a. Additionally, no significant

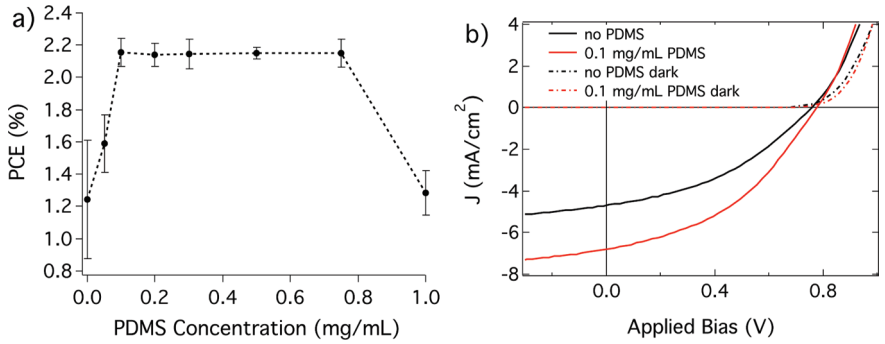

Figure 1. PCE vs PDMS concentration (a) and current density vs voltage plot for a device with no PDMS and with 0.1 mg/mL PDMS under illumination with solar simulated light (solid lines) and in the dark (dashed lines) (b) for **1-EtHx**:$PC_{61}BM$ devices after annealing at 100 °C for 20 min.

Table 1. Device Characteristics with Different Solution Concentrations of PDMS

PDMS concentration (mg/mL)	J_{SC} (mA/cm^2)[a]	V_{OC} (V)[b]	FF[c]	PCE (%)[d]
0.00	4.28	0.75	0.38	1.25 ± 0.37
0.05	6.14	0.71	0.37	1.59 ± 0.18
0.10	6.82	0.77	0.41	2.16 ± 0.09
0.20	6.51	0.77	0.43	2.14 ± 0.07
0.30	6.41	0.77	0.43	2.14 ± 0.09
0.50	6.36	0.78	0.43	2.15 ± 0.03
0.75	6.70	0.78	0.41	2.15 ± 0.09
1.0	5.95	0.68	0.32	1.28 ± 0.14

[a] J_{SC} is the short-circuit current density, [b] V_{OC} is the open-circuit voltage, [c] FF is the fill factor, [d] PCE values are listed along with the standard deviations associated with 8 cells.

difference in absorbance intensity or spectra is observed between devices with and without PDMS. Incident photon-to-current efficiency (IPCE) measurements were also performed and indicate a 37% relative increase in the average IPCE between 350 and 700 nm for a solar cell containing 0.3 mg/mL PDMS relative to a cell with no PDMS (Figure 2b). The IPCE data generally follows the film absorbance spectra with a fairly flat and broad response with the IPCE remaining between 20−29% and 29−39% from 350 to 650 nm for the devices with 0.0 and 0.3 mg/mL PDMS, respectively. Integrated IPCE values agree to within 7% of the short-circuit current values measured under simulated AM1.5 illumination.

To investigate the effect of PDMS on film morphology, we utilized atomic force microscopy (AFM) to characterize the film surfaces. The AFM images show a reduction in feature size as the PDMS concentration is increased from 0 to 0.1 mg/mL (Figure 3a−c). This reduction in feature size likely corresponds to smaller donor and acceptor phases, thus increasing the probability of an exciton reaching a D−A interface and being dissociated. As would be expected for cells with increased exciton dissociation, a corresponding increase in current density is observed. Figure 3d shows that at higher PDMS concentrations larger features begin to appear; however, no decrease in efficiency is observed at this concentration and TEM images show that small features remain underneath these larger features (see the Supporting Information, Figure S5).

Previously, it has been proposed that solvent additives function through selectively solubilizing PCBM and thus causing the polymer to become aggregated and more ordered during film drying.[26,27] This mechanism does not apply to the use of PDMS, as neither $PC_{61}BM$ nor **1-EtHx** is soluble in PDMS. It is possible that the mechanism for the improved morphology upon PDMS addition is similar to the addition of a poor solvent to the poly(3-hexylthiophene):$PC_{61}BM$ system demonstrated by Moulé et al., where the poor solvent acts to increase aggregation.[32] However, given the low concentrations of PDMS employed, it is difficult to relate this with the poor solvent example, where the poor solvent comprised 0.33 to 6.25% of the solution volume.[32] If PDMS is functioning as a poor solvent and increasing aggregation/nucleation, the increase must be in the rate of nucleation site formation, as opposed to an increase in the rate of aggregate/crystal growth, to account for the smaller domains observed. A more comprehensive study to further investigate the influence of PDMS and other solvent additives on film morphology is currently underway and will be the subject of a later publication.

It has been shown that the use of solvent additives can reduce or eliminate the need for thermal annealing.[9,26,32] To determine if this effect also applies to these materials, we characterized the device performance of **1-EtHx**:$PC_{61}BM$ solar cells with and without 0.3 mg/mL PDMS after annealing at various temperatures. It is shown in Figure 4 that without thermal annealing the PCE of the PDMS containing device is ∼5 times higher than the device containing no PDMS. As the annealing temperature is increased to 100 °C the efficiencies of both devices increase, with the PDMS containing devices remaining at least 70% more efficient than the devices without PDMS. After annealing at 120 °C, the efficiencies of both devices drop slightly and the efficiencies become more similar.

The film morphologies of the **1-EtHx**:$PC_{61}BM$ devices annealed at different temperatures were characterized through AFM as shown in Figure 5. The most significant difference can be observed between the devices with and without PDMS prior to annealing. The nonannealed device without PDMS shows large, less defined features, where as the nonannealed device with 0.3 mg/mL PDMS shows small, more well-defined features. Because of the smaller domain sizes present in the PDMS containing device, excitons are more likely to reach a D−A interface and be dissociated. As the annealing temperature is increased the morphologies of both devices become better defined with increasing feature sizes; however, the features of the PDMS containing devices remain smaller at all annealing temperatures. The more highly defined domains observed upon addition of PDMS or increasing annealing temperature correlate with a more ordered morphology, thus leading to better charge transport properties and higher device efficiencies. After annealing

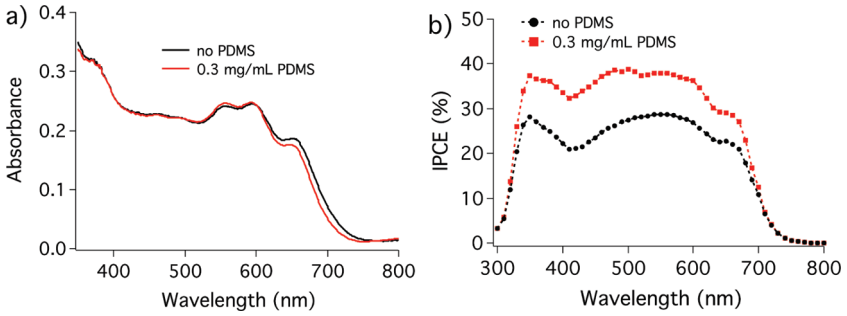

Figure 2. Absorbance spectra (a) and IPCE plot (b) for **1-EtHx**:PCBM blend films with and without PDMS.

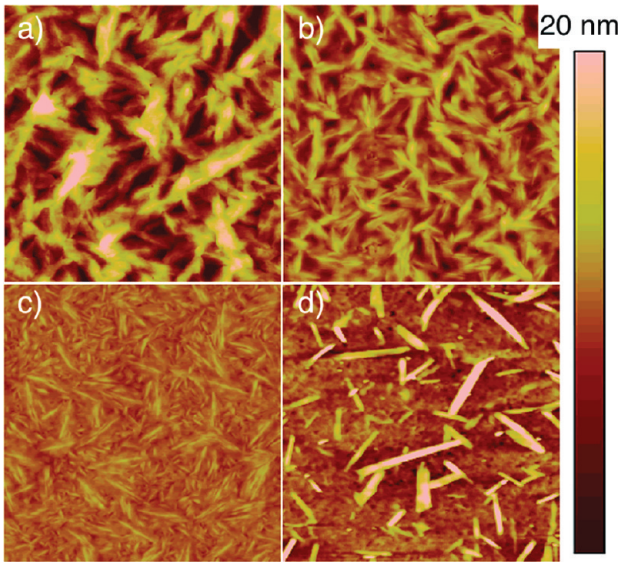

Figure 3. AFM images of **1-EtHx**:$PC_{61}BM$ with 0.00 (a), 0.05 (b), 0.1 (c), and 0.5 (d) mg/mL PDMS after annealing at 100 °C for 20 min. All images are 5 × 5 μm.

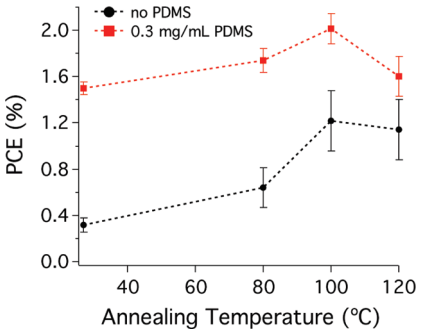

Figure 4. PCE of **1-EtHx**:$PC_{61}BM$ with no PDMS and with 0.3 mg/mL PDMS after annealing at various temperatures.

at 120 °C, the feature sizes of devices with and without PDMS become more comparable, which correlates well with the more similar efficiencies. TEM was also used to image the films and the results indicate the same trend as the AFM images, where a decrease in feature size is observed upon addition of PDMS and an increase in feature size is observed upon annealing (see the Supporting Information, Figure S6).

In addition to studying the effect of PDMS on the performance of **1-EtHx**:$PC_{61}BM$ solar cells, we also examined the effect of PDMS on **1-C7**:$PC_{61}BM$ solar cells (see the Supporting Information, Figure S7). The use of linear side chains as compared to branched EtHx side chains has a drastic effect on device morphology and leads to a significantly lower PCE. It is suspected that the linear C7 side chains allow for better intermolecular packing as well as possible intercalation of $PC_{61}BM$ between the side chains.[34] This results in features which are hundreds of nanometers in size and show no clear evidence of phase separation between **1-C7** and $PC_{61}BM$. Although significantly less efficient than the **1-EtHx** devices, it is shown that the addition of PDMS leads to a substantial increase in PCE (see Figure S7 in the Supporting Information). Similar to the **1-EtHx**:$PC_{61}BM$ cells, AFM and TEM images of the **1-C7**:$PC_{61}BM$ cells indicate a decrease in feature size upon the addition of PDMS (see the Supporting Information, Figure S8). These results suggest that the use of PDMS to improve BHJ film morphology and efficiency may be applicable to other molecular BHJ systems.

In summary, it is shown that plastic syringes can contain PDMS, which can have a significant impact on solar cell performance. For the **1-EtHx**:$PC_{61}BM$ system the addition of PDMS results in an increase in PCE from 1.25% with no PDMS to ~2.15% with 0.1−0.75 mg/mL PDMS. This increased efficiency is attributed to an improvement in all of the device characteristics, with the largest improvement in current density. Through AFM it is shown that the improved device performance results from a more favorable morphology, with PDMS containing devices displaying smaller features. Furthermore, the addition of PDMS significantly reduces the need for thermal annealing, with nonannealed devices displaying a PCE of 0.3% with no PDMS and 1.5% with 0.3 mg/mL PDMS. Again, this increased efficiency is attributed largely to the smaller, more well-defined features in the PDMS containing devices. The improvement of PCE upon addition of PDMS is also shown to apply to **1-C7**:$PC_{61}BM$ devices, which suggests that the phenomena may be applied to, other BHJ systems.

EXPERIMENTAL SECTION

Synthetic Details. Details on the synthesis of **1-EtHx** are as reported elsewhere.[33]

(E)-6,6′-Dibromo-1,1′-diheptyl-[3,3′-biindolinylidene]-2,2′-dione (6,6′-(N,N′-heptyl)-dibromoisoindigo). To a suspension of 6,6′-dibromoisoindigo (1.39 g, 3.31 mmol) and potassium carbonate (2.74 g, 19.85 mmol) in DMF (15 mL), 1-bromo-heptane (1.78 g, 9.93 mmol) was injected through a septum under nitrogen. The mixture was stirred for 15 h at 100 °C and then poured into water (200 mL). The organic phase was extracted by CH_2Cl_2, washed with brine and dried over $MgSO_4$. After removal of the solvent under reduced pressure, the pink-red solids were purified by silica chromatography, eluting with (CH_2Cl_2:

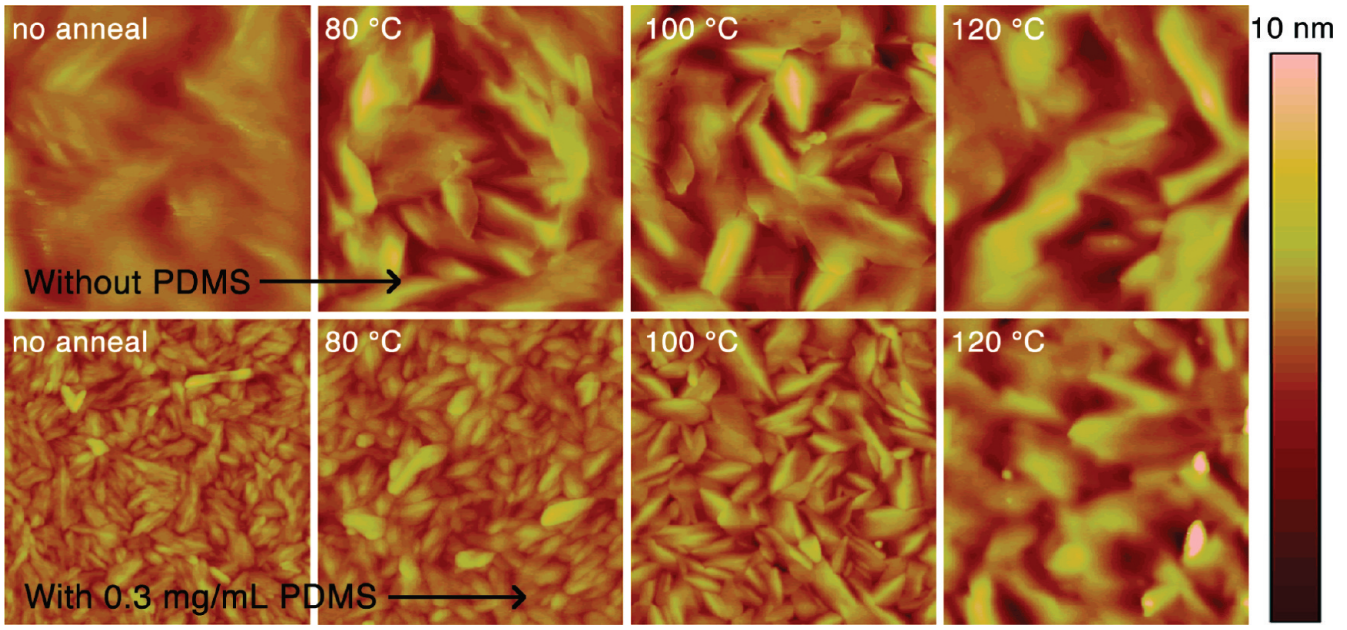

Figure 5. AFM images of **1-EtHx**:$PC_{61}BM$ with no PDMS (top) and with 0.3 mg/mL PDMS (bottom) at increasing annealing temperatures. All images are 1 × 1 μm.

Hexane =1:1) to give 6,6′-dibromo-N,N′-(heptyl)-isoindigo (1.74 g, 85%). ^{1}H NMR (300 MHz, $CDCl_3$, δ): 9.07 (d, J = 9 Hz, 2H), 7.17 (dd, J1 = 9 Hz, J2 = 1.8 Hz, 2H), 6.91 (d, J = 1.8 Hz, 2H), 3.71 (t, J = 7.2 Hz, 4H), 1.75−1.60 (m, 4H), 1.40−1.20 (m, 16H), 0.87 (t, J = 6.6 Hz, 6H); ^{13}C NMR (75 MHz, $CDCl_3$, δ): 167.9, 146.0, 132.9, 131.4, 127.0, 125.3, 120.6, 111.5, 40.5, 31.9, 29.2, 27.6, 27.2, 22.8, 14.3. HRMS (ESI-TOF) Calculated for $C_{30}H_{36}Br_2N_2O_2$ (M+H)+: 617.1198 Found: *m/z* 617.1201; Anal. Calcd for $C_{30}H_{36}Br_2N_2O_2$: C, 58.45; H, 5.89; N, 4.54; Found: 58.56; H, 5.78; N, 4.61.

(E)-1,1′-Diheptyl-6,6′-bis(5′-hexyl-[2,2′-bithiophen]-5-yl)-[3,3′-biindolinylidene]-2,2′-dione. In a flame-dried Schlenk flask (50 mL), 6,6′-(N,N′-heptyl)-dibromoisoindigo (616 mg, 1 mmol), 2-(5′-hexyl-2,2′-bithiophen-5-yl)-4,4,5,5-tetramethyl-1,3,2-dioxaborolane (904 mg, 2.4 mmol, 2.4 equiv), Tris(dibenzylideneacetone)dipalladium(0) (15 mg) and P(o-tyl)3 (10 mg) were added. The flask was evacuated and backfilled with argon three times, after which degassed toluene (20 mL) and tetraethylammonium hydroxide (3 mmol, 1M) was transferred to the mixture through a septum. The resulting solution was heated up to 85 °C under argon and stirred for 20 h. The solvent was removed under reduced pressure. The dark red solids were purified by silica gel chromatography, eluting with CH_2Cl_2-hexane (1:1) to give metallic crystalline solids (795 mg, 83%). ^{1}H NMR (300 MHz, $CDCl_3$,δ): 9.11 (d, J = 8.4, 2H), 7.24 (d, J = 3.6 Hz, 2H), 7.19(dd, J1 =8.4 Hz, J2 =1.8 Hz, 2H), 7.03 (d, J =3.6 Hz, 2H), 7.00 (d, J =3.6 Hz, 2H), 6.79 (d, J = 1.8 Hz, 2H) 6.68 (d, J =3.6 Hz, 2H), 3.74 (t, J = 4.2 Hz, 4H), 2.78 (t, J = 7.8 Hz, 4H), 1.75−1.63 (m, 8H), 1.44−1.24 (m, 28H), 0.95−0.82 (m, 12H) ^{13}C NMR (75 MHz, $CDCl_3$,δ): 168.4, 146.2, 145.3, 142.1, 138.9, 137.5, 134.7, 131.7, 130.6, 125.2, 125.1, 124.1, 123.9, 121.1, 118.9, 104.3, 40.2, 32.0, 31.8, 30.5, 29.2, 29.0, 27.8, 27.3, 22.9, 22.8, 14.3. HRMS (ESI-TOF) Calculated for $C_{58}H_{70}N_2O_2S_4$ (M+H)+: 955.4393 Found: *m/z* 955.4382. Anal. Calcd for $C_{58}H_{70}N_2O_2S_4$: C, 72.91; H, 7.38; N, 2.93. Found: C, 72.93; H,7.51; N, 3.06.

Device Fabrication. Photovoltaic devices were fabricated on 25 × 25 mm prepatterned ITO coated glass substrates (sheet resistance =15 Ω/□) with a layered structure of ITO/PEDOT:PSS/**1-EtHx** or **1-C7**:PC61BM (1:1) blend(~80 nm)/Ca(10 nm)/Al(100 nm). The ITO coated glass substrates were cleaned by sonicating sequentially in a surfactant solution, Milli-Q filtered deionized water, acetone, and isopropanol for 15 min each. The substrates were then oxygen plasma cleaned for 20 min, spin coated with PEDOT:PSS (Baytron P VP Al4083) at 5000 rpm, and dried under argon for 20 min at 120 °C. Separate solutions consisting of **1-EtHx**, **1-C7**, or $PC_{61}BM$ (SES Research) were prepared in deoxygenated anhydrous chlorobenzene (Sigma-Aldrich) at 20 mg mL^{-1} and stirred overnight in an argon filled MBraun glovebox with <0.1 ppm H_2O and O_2. A solution of poly(dimethylsiloxane) (trimethylsiloxy terminated, 14,000 MW, purchased from Alfa Aesar) was also prepared at 10 mg mL^{-1} in chlorobenzene and stirred overnight in Ar filled glovebox. Solutions were combined to form **1-EtHx** or **1-C7**:PCBM (1:1) solutions (20 mg mL^{-1}) with varying PDMS concentration and stirred 1 h at 60 °C. The solutions were filtered with 0.2 μm PTFE filters using clean glass syringes, spin coated at 1000 rpm, and annealed on a hot plate in an argon atmosphere at the indicated temperature for 20 min. The thermal deposition of the calcium (10 nm) and aluminum (100 nm) electrode was performed at 10^{-6} mbar through a shadow mask that defined 8 individually addressable 3 mm diameter cells (0.071 cm^2) per 25 × 25 mm substrate. Photovoltaic performance was characterized under illumination with an AM1.5 filtered Xe arc lamp at 100 mW/cm^2 in an argon atmosphere (<0.1 ppm H_2O and O_2) through current−voltage curves recorded with a Keithley 2400 source meter. For all given plots the data included is all from the same set of devices (devices made at the same time) to minimize the effects of set-to-set variation. IPCE characterization was performed with a Xe arc lamp fitted with a monochromator, the intensity was measured at each wavelength increment with a calibrated Si photodiode (UDT Instruments), and a Keithley 2400 source meter was used with 0 voltage bias to record the current at each illumination wavelength. Device sets with varying concentrations of PDMS and annealed at 100 °C (same as indicated in figure 1) were made on 4 different occasions with nearly identical results achieved for each device set. For devices made in the Kippelen laboratory conditions were identical with the following exceptions: pixel size (0.097 to 0.130 cm^2) and location differed from Reynolds laboratory devices, chlorobenzene was anhydrous but not deoxygenated, $PC_{61}BM$ was from nano-C, and ITO was patterned by depositting a layer of SiO_X to create a nonconductive region. For devices made in the So laboratory conditions were identical

with the following exceptions: ITO substrates were exposed to UV ozone in place of oxygen plasma, pixel size (0.045 cm^2) and location differed from Reynolds lab devices, chlorobenzene was anhydrous but not deoxygenated, a nitrogen atmosphere glovebox was used with H_2O ~5.0 ppm during device fabrication, 1 nm LiF was deposited in place of 10 nm Ca, and devices were measured in the ambient atmosphere.

Morphology Characterization. AFM was performed with a Veeco Innova scanning probe microscope in tapping mode using MikroMasch NSC15 tips with a resonant frequency ~325 kHz and a force constant ~40 N/m. All AFM images were taken within 3 mm of a cell. TEM was performed in bright field mode at an accelerating voltage of 200 kV using either a JEOL 200CX or a JEOL 2010F TEM.

■ ASSOCIATED CONTENT

Supporting Information. Information includes plastic vs glass syringe illuminated *J*−*V* plot, IR and MALDI-MS spectra of a PDMS standard and plastic syringe extract, solar cell data from So and Kippelen laboratories, TEM images, and AFM images of the **1-C7**:$PC_{61}BM$ films (PDF). This material is available free of charge via the Internet at http://pubs.acs.org.

■ AUTHOR INFORMATION

Corresponding Author
*E-mail: fso@mse.ufl.edu (F.S.); kippelen@ece.gatech.edu (B.K.); reynolds@chem.ufl.edu (J.R.R).

■ ACKNOWLEDGMENT

We gratefully acknowledge the AFOSR (FA9550-09-1-0320) for financial support. K.R.G. and R.S. acknowledge the University Alumni Awards Program for a fellowship. F.S. acknowledges the support of Florida Energy Systems Consortium. B.K., J.W.S., and H.C. acknowledge partial support through the STC Program of the National Science Foundation (B.K.) under Agreement DMR-0120967, and the Center for Interface Science: Solar Electric Materials, an Energy Frontier Research Center funded by the U.S. Department of Energy, Office of Science, Office of Basic Energy Sciences, under Award DE-SC0001084 (J.W.S., H.C.). We acknowledge Kerry N. Siebein and the Major Analytical Instrumentation Center, Department of Materials Science and Engineering, University of Florida, for TEM facility use and assistance. We also acknowledge Kyle Anne Lunsford and Dr. Rick Yost for their MALDI-MS analysis of the PDMS sample, and Dr. Willliam Potscavage Jr. and Dr. Denke Cai for their assistance during device fabrication.

■ REFERENCES

(1) Morton, O. *Nature* **2006**, *443*, 19–22.
(2) Brabec, C. J.; Sariciftci, N. S.; Hummelen, J. C. *Adv. Funct. Mater.* **2001**, *11*, 15–26.
(3) Ma, W.; Yang, C.; Gong, X.; Lee, K.; Heeger, A. J. *Adv. Funct. Mater.* **2005**, *15*, 1617–1622.
(4) Thompson, B. C.; Frechet, J. M. J. *Angew. Chem., Int. Ed.* **2008**, *47*, 58–77.
(5) Chen, H. Y.; Hou, J. H.; Zhang, S. Q.; Liang, Y. Y.; Yang, G. W.; Yang, Y.; Yu, L. P.; Wu, Y.; Li, G. *Nat. Photonics* **2009**, *3*, 649–653.
(6) Walker, B.; Tomayo, A. B.; Dang, X. D.; Zalar, P.; Seo, J. H.; Garcia, A.; Tantiwiwat, M.; Nguyen, T. Q. *Adv. Funct. Mater.* **2009**, *19*, 3063–3069.
(7) Krebs, F. C.; Gevorgyan, S. A.; Alstrup, J. *J. Mater. Chem.* **2009**, *19*, 5442–5451.
(8) Li, G.; Yao, Y.; Yang, H.; Shrotriya, V.; Yang, G.; Yang, Y. *Adv. Funct. Mater.* **2007**, *17*, 1636–1644.
(9) Peet, J.; Kim, J. Y.; Coates, N. E.; Ma, W. L.; Moses, D.; Heeger, A. J.; Bazan, G. C. *Nat. Mater.* **2007**, *6*, 497–500.
(10) Kim, J. Y.; Lee, K.; Coates, N. E.; Moses, D.; Nguyen, T. Q.; Dante, M.; Heeger, A. J. *Science* **2007**, *317*, 222–225.
(11) Tamayo, A. B.; Walker, B.; Nguyen, T. Q. *J. Phys. Chem. C* **2008**, *112*, 11545–11551.
(12) Silvestri, F.; Irwin, M. D.; Beverina, L.; Facchetti, A.; Pagani, G. A.; Marks, T. J. *J. Am. Chem. Soc.* **2008**, *130*, 17640–17641.
(13) Winzenberg, K. N.; Kemppinen, P.; Fanchini, G.; Bown, M.; Collis, G. E.; Forsyth, C. M.; Hegedus, K.; Singh, T. B.; Watkins, S. E. *Chem. Mater.* **2009**, *21*, 5701–5703.
(14) Zhang, J.; Yang, Y.; He, C.; He, Y. J.; Zhao, G. J.; Li, Y. F. *Macromolecules* **2009**, *42*, 7619–7622.
(15) Li, W. W.; Du, C.; Li, F. H.; Zhou, Y.; Fahlman, M.; Bo, Z. S.; Zhang, F. L. *Chem. Mater.* **2009**, *21*, 5327–5334.
(16) Tamayo, A. B.; Dang, X. D.; Walker, B.; Seo, J.; Kent, T.; Nguyen, T. Q. *Appl. Phys. Lett.* **2009**, *94*, 103301.
(17) Mikroyannidis, J. A.; Sharma, S. S.; Vijay, Y. K.; Sharma, G. D. *ACS Appl. Mater. Interfaces* **2009**, *2*, 270–278.
(18) Velusamy, M.; Huang, J. H.; Hsu, Y. C.; Chou, H. H.; Ho, K. C.; Wu, P. L.; Chang, W. H.; Lin, J. T.; Chu, C. W. *Org. Lett.* **2009**, *11*, 4898–4901.
(19) Fan, H. J.; Shang, H. X.; Li, Y. F.; Zhan, X. W. *Appl. Phys. Lett.* **2010**, *97*, 133302.
(20) Zhang, J.; Deng, D.; He, C.; He, Y.; Zhang, M.; Zhang, Z.-G.; Zhang, Z.; Li, Y. *Chem. Mater.* **2011**, *23*, 817–822.
(21) Gunes, S.; Neugebauer, H.; Sariciftci, N. S. *Chem. Rev.* **2007**, *107*, 1324–1338.
(22) Scully, S. R.; McGehee, M. D. *J. Appl. Phys.* **2006**, *100*, 034907.
(23) Shaw, P. E.; Ruseckas, A.; Samuel, I. D. W. *Adv. Mater.* **2008**, *20*, 3516–3520.
(24) Savenije, T. J.; Kroeze, J. E.; Yang, X.; Loos, J. *Adv. Funct. Mater.* **2005**, *15*, 1260–1266.
(25) Miller, S.; Fanchini, G.; Lin, Y. Y.; Li, C.; Chen, C. W.; Su, W. F.; Chhowalla, M. *J. Mater. Chem.* **2008**, *18*, 306–312.
(26) Yao, Y.; Hou, J. H.; Xu, Z.; Li, G.; Yang, Y. *Adv. Funct. Mater.* **2008**, *18*, 1783–1789.
(27) Lee, J. K.; Ma, W. L.; Brabec, C. J.; Yuen, J.; Moon, J. S.; Kim, J. Y.; Lee, K.; Bazan, G. C.; Heeger, A. J. *J. Am. Chem. Soc.* **2008**, *130*, 3619–3623.
(28) Chen, F. C.; Tseng, H. C.; Ko, C. J. *Appl. Phys. Lett.* **2008**, *92*, 103316.
(29) Hoven, C. V.; Dang, X. D.; Coffin, R. C.; Peet, J.; Nguyen, T. Q.; Bazan, G. C. *Adv. Mater.* **2010**, *22*, E63–E66.
(30) Dante, M.; Garcia, A.; Nguyen, T. Q. *J. Phys. Chem. C* **2009**, *113*, 1596–1600.
(31) Pivrikas, A.; Stadler, P.; Neugebauer, H.; Sariciftci, N. S. *Org. Electron.* **2008**, *9*, 775–782.
(32) Moulé, A. J.; Meerholz, K. *Adv. Mater.* **2008**, *20*, 240–245.
(33) Mei, J. G.; Graham, K. R.; Stalder, R.; Reynolds, J. R. *Org. Lett.* **2010**, *12*, 660–663.
(34) Mayer, A. C.; Toney, M. F.; Scully, S. R.; Rivnay, J.; Brabec, C. J.; Scharber, M.; Koppe, M.; Heeney, M.; McCulloch, I.; McGehee, M. D. *Adv. Funct. Mater.* **2009**, *19*, 1173–1179.